How should the optical tweezers experiment be used to characterize the red blood cell membrane mechanics?

Julien Sigüenza, Simon Mendez, Franck Nicoud

How should the optical tweezers experiment be used to characterize the red blood cell membrane mechanics?

Julien Sigüenza[1,2] · **Simon Mendez**[1] · **Franck Nicoud**[1]

Abstract Stretching red blood cells using optical tweezers is a way to characterize the mechanical properties of their membrane by measuring the size of the cell in the direction of the stretching (axial diameter) and perpendicularly (transverse diameter). Recently, such data have been used in numerous publications to validate solvers dedicated to the computation of red blood cell dynamics under flow. In the present study, different mechanical models are used to simulate the stretching of red blood cells by optical tweezers. Results first show that the mechanical moduli of the membranes have to be adjusted as a function of the model used. In addition, by assessing the area dilation of the cells, the axial and transverse diameters measured in optical tweezers experiments are found to be insufficient to discriminate between models relevant to red blood cells or not. At last, it is shown that other quantities such as the height or the profile of the cell should be preferred for validation purposes since they are more sensitive to the membrane model.

Keywords Red blood cells · Optical tweezers · Membrane modeling · Cytoskeleton · Lipid bilayer · Fluid–structure interactions · Immersed boundary method

✉ Julien Sigüenza
j.siguenza@sim-and-cure.com

[1] Institut Montpelliérain Alexander Grothendieck (IMAG), CNRS, Université de Montpellier, 2 Place Eugène Bataillon, 34095 Montpellier Cedex 5, France

[2] Sim and Cure, Cap Gamma, 1682 rue de la Valsière, 34790 Grabels, France

1 Introduction

Blood is a complex substance consisting in a suspension of platelets, white blood cells and red blood cells (RBCs) in a Newtonian fluid, the plasma. The RBCs, which typically represent 40–45% of the whole blood volume, are composed of a membrane enclosing an internal fluid, the cytoplasm. The RBC membrane is a composite structure composed of a lipid bilayer and a two-dimensional elastic cytoskeleton, both linked through temporary tethering sites thanks to transmembrane proteins embedded in the lipid bilayer. This complex structure confers to the RBC membrane very specific mechanical properties: The cytoskeleton provides a resistance to shear solicitations and slightly resists to area dilatation, while the lipid bilayer provides to the membrane its bending stiffness and quasi-incompressibility. The RBCs have a biconcave discocyte shape at rest with a remarkable deformability, because of the excess of surface area enclosing the inner volume. RBCs are thus able to undergo very large deformation preserving their area, squeezing through capillaries with inner diameter less than 3 μm, although the average large diameter of a RBC is about 8 μm. As mentioned by Mohandas and Gallagher (2008), the normal RBC can deform with linear extensions of up to 250%, but a 3–4% increase in surface area results in cell lysis.

So far, there is no universal model to describe the mechanical behavior of the RBC membrane. The local elasticity of the RBC membrane is generally described using either continuum models (Le et al. 2009; Klöppel and Wall 2011; Farutin et al. 2014; Sinha and Graham 2015) or network models (Li et al. 2005; Dao et al. 2006; Pivkin and Karniadakis 2008; Fedosov et al. 2010a, b, 2014; Chen and Boyle 2014), which can be complemented with other global models to treat the quasi-incompressibility of the lipid bilayer (Pivkin and Karniadakis 2008; Fedosov et al. 2010a, b). Detailed experi-

mental investigations of the RBC mechanics are nonetheless needed in order to: (1) characterize and validate a numerical model of the RBC membrane and (2) once validated, determine the mechanical parameters of the model.

To gain insight into the mechanical behavior of RBCs, experimental techniques were developed for measurements of the RBC membrane properties (Abkarian and Viallat 2016). Micropipette aspiration (Evans 1973) and optical tweezers (Hénon 1999; Mills et al. 2004) are the most popular ones and were notably used to determine the shear modulus of the RBC membrane. The optical tweezers experiment by Mills et al. (2004) provides a useful means for the analysis of the single cell mechanics under a variety of well-controlled stress states, where stretching of an isolated RBC is generated by means of attached silica microbeads and optical trap. Using a continuum model of the RBC membrane to solve the deformation of the RBC subjected to optical stretching, Yeoh (1993) successfully matched the force-extension data obtained from the experiment, thus enabling the extraction of the shear modulus of the RBC membrane.

A recent work of Dimitrakopoulos (2012) showed that large differences of shear modulus reported in various studies may be explained based on the different membrane models used to fit the experimental data. Theoretically investigating continuum models under uniaxial extension and local area incompressibility, he showed that the only constitutive law able to properly match the wide variety of experimental data available in the literature is the Skalak law, specifically developed by Skalak et al. (1973) to represent the in-plane elasticity of the RBC membrane. Based on this finding, Dimitrakopoulos stated that Mills et al. (2004) found the shear modulus that represents the Yeoh law, but not the true shear modulus of the RBC membrane. This purely theoretical work was specifically dedicated to the response of different membrane laws under small, moderate and large shear strains. A more realistic configuration where the whole RBC is stretched as in the Mills et al. (2004) experiment was, however, not considered by Dimitrakopoulos (2012); this is done computationally in the present paper.

As a consequence, the numerical results of Mills et al. (2004) were successfully matched to the force-extension data obtained from optical tweezers using the Yeoh law, whereas a proper modeling of the RBC membrane should rather rely on the Skalak law. This reveals the simplistic nature of these experimental data, which was also pointed out by Dimitrakopoulos (2012). Despite this observation, optical tweezers data continue to be used as a way to validate numerical models of the RBC membrane (Li et al. 2005; Dao et al. 2006; Pivkin and Karniadakis 2008; Le et al. 2009; Fedosov et al. 2010a, b, 2014; Klöppel and Wall 2011; Chen and Boyle 2014; Farutin et al. 2014; Sinha and Graham 2015), notably to probe the accuracy of solvers dedicated to the study of the RBC dynamics under flow. However, a proper validation test case needs to be selective to discriminate between appropriate and inappropriate models. There is a suspicion that computing optical tweezers experiment does not constitute a true validation test case.

The present paper constitutes a numerical study which first aims at emphasizing previous findings of Dimitrakopoulos (2012), highlighting the limitations of the optical tweezers experiment for characterizing the mechanics of the RBC membrane. Theoretical investigations of Dimitrakopoulos (2012) are here complemented with detailed simulations of the optical tweezers experiment by Mills et al. (2004), using a numerical method dedicated to the simulation of the dynamics of RBCs under flow. After a brief description of this numerical method, an easy-to-implement computational setup is presented and validated against the numerical results of Mills et al. (2004). Then, different continuum membrane models are investigated, based on various combinations of strain, area conservation and bending energies. If the membrane incompressibility can be easily imposed theoretically (Dimitrakopoulos 2012), it is rarely done in models of red blood cells. The membrane is generally modeled using a mechanical resistance to area dilatation, which enables some small area variation of the membrane (Li et al. 2005; Dao et al. 2006; Pivkin and Karniadakis 2008; Fedosov et al. 2010a, b, 2014; Chen and Boyle 2014; Sinha and Graham 2015). In the present study, the impact of this area dilatation resistance is carefully investigated, restraining the area variation of the membrane either locally or globally. Detailed analysis of the shape of the stretched RBC are also carried out in order to identify which kind of additional experimental data could be helpful to better characterize the mechanics of the RBC membrane.

2 Numerical method

The present numerical method is very similar to the one developed by Mendez et al. (2014) and Sigüenza et al. (2016) for fluid–structure interactions (FSI) of deformable membranes, and is based on the immersed boundary method (IBM) introduced by Peskin (2002). Two independent meshes are considered to discretize the RBC membrane and the fluid. The RBC membrane is discretized by a moving Lagrangian mesh, and the fluid is discretized by a fixed Eulerian unstructured mesh. The different steps of the present method are the following:

(1) The membrane force $\vec{F}$ is calculated on the Lagrangian mesh, which depends on the membrane deformation and on the models used to represent the membrane rheology.
(2) The forces exerted by the membrane on the fluid are represented by the fluid volumetric force $\vec{f}$, calculated on the Eulerian mesh by regularizing the membrane force $\vec{F}$ such as

$$\overrightarrow{f}\left(\overrightarrow{x},t\right)=\int_{\Omega_s}\overrightarrow{F}\left(\overrightarrow{X},t\right)\delta\left(\overrightarrow{x}-\overrightarrow{X}\right)\mathrm{d}X,$$

where $\overrightarrow{x}$ and $\overrightarrow{X}$, respectively, denote the coordinates vectors of the Eulerian fluid nodes and Lagrangian nodes, Ω_s denotes the solid domain defining the RBC membrane and δ is the well-known Dirac function.

(3) The fluid velocity $\overrightarrow{v}$ is calculated on the Eulerian mesh by solving the Navier–Stokes equations (forced by the source term $\overrightarrow{f}$).

(4) The membrane velocity $\overrightarrow{V}$ is calculated on the Lagrangian mesh by interpolating the fluid velocity $\overrightarrow{v}$ such as

$$\overrightarrow{V}\left(\overrightarrow{X},t\right)=\int_{\Omega_f}\overrightarrow{v}\left(\overrightarrow{x},t\right)\delta\left(\overrightarrow{x}-\overrightarrow{X}\right)\mathrm{d}X,$$

where Ω_f denotes the fluid domain.

The Dirac function δ used in the procedures of regularization and interpolation of steps (2) and (4) is numerically represented by a smooth discrete Dirac function, which is adapted to unstructured meshes using the Reproducing Kernel particle method (Pinelli et al. 2010; Mendez et al. 2014; Sigüenza et al. 2016). Interpolation of the fluid velocity on the membrane Lagrangian mesh leads to small mass conservation errors. A specific algorithm has been developed to perfectly conserve the volume of the RBC during the calculations (Mendez et al. 2014; Sigüenza et al. 2016).

2.1 Membrane forces computation

In the present method, the RBC membrane is considered to be infinitely thin and is represented by a triangulated surface. The membrane force is derived from a combination of strain, area conservation and bending energies. Resistances to shear and area dilatation are modeled thanks to a hyperelastic strain energy function W, which is written as a function of the local in-plane principal values of strain λ_1 and λ_2, following the method of Charrier et al. (1989), Eggleton and Popel (1998), Sui et al. (2008) and Doddi and Bagchi (2008). Several hyperelastic models are investigated in the present study:

- The neo-Hookean law,

$$W_{\mathrm{NH}}=\frac{E_s}{2}\left(\lambda_1^2+\lambda_2^2+\lambda_1^{-2}\lambda_2^{-2}-3\right), \tag{1}$$

where E_s stands for the membrane in-plane shear modulus.

- The Yeoh law,

$$W_{\mathrm{YE}}=\frac{E_s}{2}\left(\lambda_1^2+\lambda_2^2+\lambda_1^{-2}\lambda_2^{-2}-3\right)+C_3\left(\lambda_1^2+\lambda_2^2+\lambda_1^{-2}\lambda_2^{-2}-3\right)^3, \tag{2}$$

which is an extension of the previous neo-Hookean law, with the addition of a nonlinear term driven by the nonlinear modulus C_3.

- The law introduced by Skalak et al. (1973) for red blood cells,

$$W_{\mathrm{SK}}=\frac{E_s}{4}\left[\left(\lambda_1^2+\lambda_2^2-2\right)^2+2\left(\lambda_1^2+\lambda_2^2-\lambda_1^2\lambda_2^2-1\right)\right]+\frac{E_a}{4}\left(\lambda_1^2\lambda_2^2-1\right)^2, \tag{3}$$

where shear resistance and area dilatation resistance are separately taken into account through the shear modulus E_s and the area dilatation modulus E_a, respectively. It can also be written with the ratio of the area dilatation modulus to the shear modulus, $C=E_a/E_s$,

$$W_{\mathrm{SK}}=\frac{E_s}{4}\left[\left(\lambda_1^2+\lambda_2^2-2\right)^2+2\left(\lambda_1^2+\lambda_2^2-\lambda_1^2\lambda_2^2-1\right)+C\left(\lambda_1^2\lambda_2^2-1\right)^2\right]. \tag{4}$$

Although the Skalak law can be used to control area variations of the RBC membrane, another approach consists in using a global area conservation energy:

$$\mathcal{E}_S=\frac{\kappa_S}{2}\frac{(S-S_0)^2}{S_0}, \tag{5}$$

with κ_S the area modulus, S the area of the membrane and S_0 its target area. This energy is actually already used in other formulations based on discrete approaches (Pivkin and Karniadakis 2008; Fedosov et al. 2010b) or in shape predictions by energy minimization (Lim et al. 2002, 2008). Conveniently, the force applied by the membrane on the fluid associated with the energy term $\mathcal{E}_S$ can be expressed explicitly:

$$\overrightarrow{F_S}=-2\kappa_S\frac{(S-S_0)}{S_0}H\,\overrightarrow{n}, \tag{6}$$

with H the mean curvature and $\overrightarrow{n}$ the outward normal vector to the surface.

In addition, the bending resistance of the membrane can be represented using the bending energy $\mathcal{E}_b$, proposed by Helfrich (1973):

$$\mathcal{E}_b=\frac{\kappa_b}{2}\int_S(2H-c_0)^2\,\mathrm{d}S, \tag{7}$$

Table 1 Different energies available to model the RBC membrane and associated notations of mechanical moduli

W		$\mathcal{E}_S$	$\mathcal{E}_b$
NH:	E_s (N/m)	κ_S (N/m)	κ_b (N.m)
YE:	E_s (N/m)		
	C_3 (N/m)		
SK:	E_s (N/m)		
	C		

with $\kappa_\mathrm{b} = 2.0 \times 10^{-19}$ N m (Lim et al. 2002, 2008) the bending modulus, and c_0 a possible spontaneous curvature (which is set to zero in the present study). The bending force applied by the membrane on the fluid reads:

$$\overrightarrow{F_\mathrm{b}} = \kappa_\mathrm{b} \Big[(2H - c_0) \left(2H^2 - 2K + c_0 H \right) + 2\Delta_\mathrm{LB} H \Big] \overrightarrow{n}, \tag{8}$$

where Δ_LB denotes the surface Laplacian operator (Zhongcan and Helfrich 1989) (also called the Laplace–Beltrami operator) and K is the local Gaussian curvature of the surface. The terms of the bending force are calculated by local fitting of a quadratic approximation of the surface. The method is similar to the one used by Farutin et al. (2014). Table 1 summarizes the three energies introduced, with the associated parameters. Every combination of these energies (W, $\mathcal{E}_S$, $\mathcal{E}_\mathrm{b}$) can be used to model the RBC membrane.

2.2 Navier–Stokes equations solver

The fluid inside and outside the RBC is supposed to be incompressible and Newtonian. The YALES2BIO flow solver is used (Mendez et al. 2014; Chnafa et al. 2014; Sigüenza et al. 2016; Zmijanovic et al. 2017) to solve the forced Navier–Stokes equations over the Eulerian unstructured mesh by using a projection method (Chorin 1968). The momentum conservation equations reads:

$$\frac{\partial \overrightarrow{v}}{\partial t} + \overrightarrow{\nabla} . \left(\overrightarrow{v} \otimes \overrightarrow{v} \right) = -\frac{\overrightarrow{\nabla} p}{\rho} + \nu \Delta \overrightarrow{v} + \frac{\overrightarrow{f}}{\rho}, \tag{9}$$

where $\overrightarrow{v}$ and p are the velocity vector and the pressure, ρ the density and ν the kinematic viscosity. For an incompressible fluid, the mass conservation equation becomes:

$$\overrightarrow{\nabla} . \overrightarrow{v} = 0 \tag{10}$$

The fluid velocity is advanced using a fourth-order centered scheme in space and a fourth-order Runge–Kutta scheme in time. A divergence-free velocity field is obtained at the end of the time step by solving a Poisson equation for pressure and correcting the predicted velocity. A deflated preconditioned conjugate gradient (DPCG) algorithm is used to solve this Poisson equation (Moureau et al. 2011; Malandain et al. 2013).

The YALES2BIO solver was validated in several test cases where reference data (either experimental, analytical or numerical) are available. This is described in previous publications, where the reader can also find additional implementation details (Martins Afonso et al. 2014; Mendez et al. 2014; Sigüenza et al. 2014, 2016; Zmijanovic et al. 2017).

3 Optical tweezers modeling

The purpose of this section is to establish a computational setup allowing the computation of the optical tweezers experiment by Mills et al. (2004). The computational setup presented in this section is built heavily on the one developed by Dao et al. (2003), which has also been used by Mills et al. (2004) to simulate the optical tweezers experiment.

Figure 1a illustrates the experimental setup used in Mills et al. (2004) to perform the stretching of the RBC. Two silica microbeads, of diameter 4.12 µm, are attached to the cell at diametrically opposite points. The left bead is anchored to the surface of a glass slide while the right bead is trapped by a laser beam. The trapped bead remaining at rest, moving the slide and attached left bead stretches the cell. Then, the axial diameter D_A (in the direction of the stretching), and the transverse diameter D_T (orthogonal to the stretching direction) are measured on the stretched RBC.

3.1 Computational setup

The analytical model of the RBC biconcave shape proposed by Evans and Fung (1972) is used to define the RBC geometry:

$$z = \pm 0.5 R_0 \left[1 - \frac{x^2 + y^2}{R_0^2} \right] \times \left[A_1 + A_2 \frac{x^2 + y^2}{R_0^2} + A_3 \left(\frac{x^2 + y^2}{R_0^2} \right)^2 \right] \tag{11}$$

where $R_0 = 3.91\,\mu$m is the average RBC radius, $A_1 = 0.207161$, $A_2 = 2.002558$ and $A_3 = -1.122762$.

Rather than explicitly solving the contact between the beads and the RBC (as Dao et al. 2003 and Mills et al. 2004), most of the works simulating the optical tweezers experiment consider pure Neumann loading conditions to simulate the RBC stretching, applying a constant stretching force F over a certain percentage of nodes at the extremities of the RBC

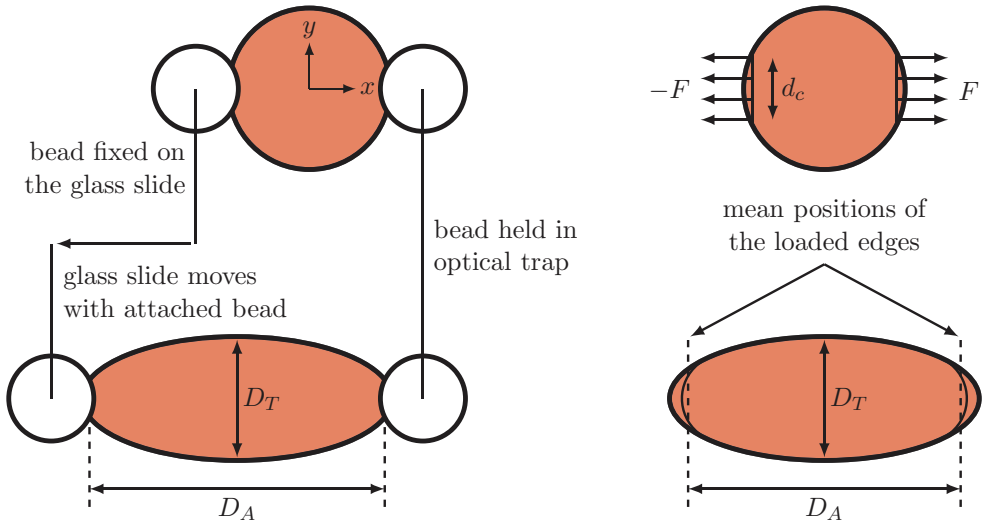

(a) Experimental setup **(b)** Computational setup

Fig. 1 **a** Illustration of the experimental setup of Mills et al. (2004). The axial (D_A) and transverse (D_T) diameters of the stretched RBC are measured. **b** Computational setup used to simulate the optical tweezers experiment. A stretching force F is applied over the two circular edges delimitating the contact areas between the RBC and the beads, with a contact size $d_c = 2\,\mu m$

(Le et al. 2009; Farutin et al. 2014; Chen and Boyle 2014; Fedosov et al. 2014; Sinha and Graham 2015). The drawback of this approach was nonetheless pointed out by Klöppel and Wall (2011): The rigidity of the beads is not properly taken into account, leading to a larger axial diameter (D_A), and thus a higher estimation of the in-plane shear modulus. An alternative methodology which mimics the beads rigidity is introduced in what follows, within a three-step strategy:

- The contact areas between the beads and the RBC are properly defined following the procedure of Dao et al. (2003). As shown in Fig. 1b, these contact areas are defined by intersecting the surface of the RBC with two opposite planes perpendicular to the stretching direction. The position of these planes is chosen such that the contact size between the beads and the RBC is $d_c = 2\,\mu m$ (Dao et al. 2003).
- Rather than applying the stretching force F over all the nodes of the contact areas, the force is applied only to the nodes located on the edges delimiting the contact areas (see Fig. 1b).
- Instead of evaluating the axial diameter (D_A) as the distance between the extremities of the stretched RBC, the axial diameter is determined by calculating the mean position of each loaded edge, which are deformed during the RBC stretching (as sketched in Fig. 1b).

Consistent with the numerical framework described in Sect. 2, the computation of the RBC stretching consists in solving a transient fluid–structure interaction problem until stabilization of the shape. The RBC is immersed in a fluid box extended from $-4R_0$ to $4R_0$ in the x direction (direction of the stretching), from $-2R_0$ to $2R_0$ in the y direction (direction orthogonal to the stretching), and from $-R_0$ to R_0 in the z direction (direction perpendicular to the plane of the RBC). The fluid mesh is composed of 881 992 tetrahedral elements, with a constant mesh resolution of $R_0/12.5$. The RBC membrane is composed of 6 434 nodes, with a constant mesh resolution of $R_0/25$.

The stretching force is applied on the RBC membrane as an external force, with a time-dependent ramp ranging from 0 to the desired value of F. This external force is seen by the fluid which starts moving, and deforms the RBC. After a transient phase, the mechanical forces inside the membrane and the applied external force balance, and a steady deformation is obtained. The choice of the fluid properties and the size of the computational domain may affect the transient phase, but have no influence on the steady deformation of the RBC and calculated axial and transverse diameters. Only the final stabilized shapes are postprocessed.

3.2 Validation

With the aim of validating the present computational setup, the optical tweezers experiment by Mills et al. (2004) is simulated, and the present simulations are compared with the numerical simulations performed by Mills et al. (2004). Two cases are simulated, corresponding to different modeling of the RBC membrane. These two cases are summarized in Table 2. For both cases, only the local in-plane elasticity is considered. The membrane is assumed to follow the neo-

Table 2 Cases simulated with the present computational setup and compared with the results of Mills et al. (2004)

	W		$\mathcal{E}_S$	$\mathcal{E}_b$
Case 1	NH:	$E_s = 7.3\ \mu$N/m	X	X
Case 2	YE:	$E_s = 7.3\ \mu$N/m $C_3 = E_s/30$	X	X

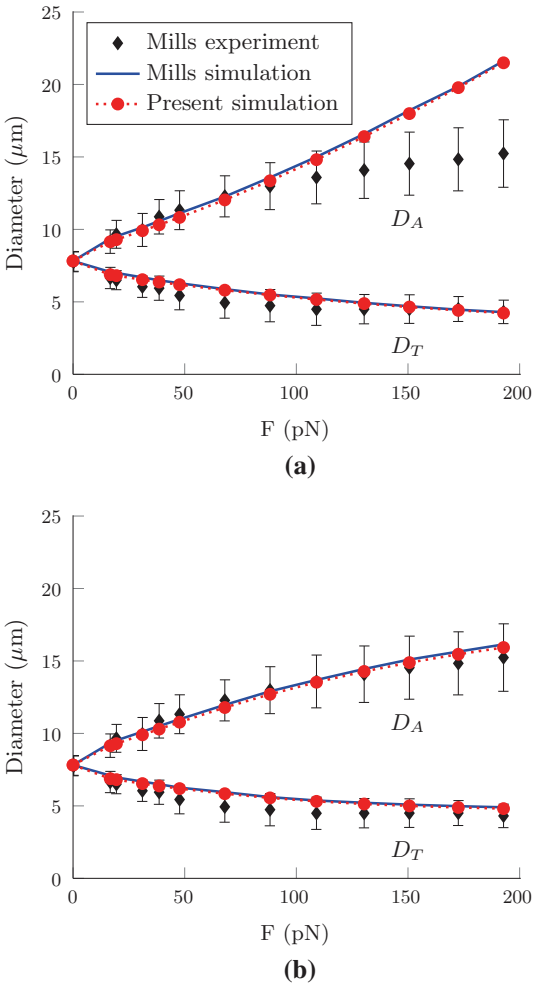

Fig. 2 Axial (D_A) and transverse (D_T) diameters of the RBC stretched by optical tweezers. Comparison with the experimental and numerical data from Mills et al. (2004). **a** The RBC membrane is assumed to follow the neo-Hookean law, corresponding to case 1. **b** The RBC membrane is assumed to follow the Yeoh law, corresponding to case 2

Hookean law (Eq. 1) in case 1, and the Yeoh law (Eq. 2) in case 2.

Figure 2 shows both axial (D_A) and transverse (D_T) diameters of the RBC stretched by optical tweezers, as a function of the applied force, for cases 1 and 2. As the cell is more and more elongated when increasing the stretching force, it is seen that the axial diameter (D_A) increases. The elongation of the cell leads to its contraction in the orthogonal direction, resulting in a decrease of the transverse diameter (D_T).

When using pure Neumann loading conditions to simulate the RBC stretching (Le et al. 2009; Farutin et al. 2014; Chen and Boyle 2014; Fedosov et al. 2014; Sinha and Graham 2015), the rigidity of the beads used in the optical tweezers experiment is not taken into account, which is known to strongly influence the deformation of the stretched RBC, especially the estimation of the axial diameter (D_A) (Klöppel and Wall 2011). The present results, however, show that it is possible to mimic the beads rigidity using a customized computational setup based on pure Neumann loading conditions, which is seen to faithfully reproduce the numerical results obtained by Mills et al. (2004), who explicitly solved the contact between the beads and the RBC.

As pointed out by Mills et al. (2004), comparison of the numerical results of case 1 with the experimental data shows that the neo-Hookean law is not adapted to describe the behavior of the RBC membrane. Indeed, experimental trends are well captured over the range of 0–88 pN. However, the model deviates gradually for loadings higher than 88 pN, showing a strain-softening behavior under large deformation (Barthès-Biesel et al. 2002). Conversely, the Yeoh law provides accurate predictions of diameters over the entire range of experimental data. The strain-hardening behavior of RBCs under large deformation is thus well transcribed by the model. Regarding the mechanical response of the stretched RBC in terms of axial (D_A) and transverse (D_T) diameters, the membrane modeling corresponding to case 2, using the Yeoh law, provides a good description of the membrane mechanical behavior.

In order to investigate the influence of the mesh resolution, two meshes were constructed from the mesh used in Fig. 2: A coarse mesh whose resolution is twice coarser than the reference mesh resolution and a fine mesh whose resolution is twice finer than the reference mesh resolution. Axial (D_A) and transverse (D_T) diameters obtained from these three meshes are compared in Table 3 with the diameters obtained from numerical simulations of Mills et al. (2004) for the largest loading $F = 193$ pN. The mesh resolution has almost no influence on the prediction of the axial diameter (D_A), and only small influence on the prediction of the transverse diameter (D_T). This indicates that the reference mesh is sufficiently refined, and can thus be used in the remainder of this study.

Figure 3 shows the deformation of the RBC for different values of the stretching force F, which ranges from 0 to 193 pN. A detailed analysis of the shape of the RBC shows that as the cell is elongated when increasing the force, a large fold is appearing, as also observed in the numerical simulations of Mills et al. (2004). Occurence of such a folding is, however, not investigated in the experiment.

Table 3 Influence of the mesh resolution for case 2, at the maximum imposed force of 193 pN

	D_A (μm)	D_T (μm)
Mills simulation	16.14	4.90
Coarse mesh	15.92	4.94
Reference mesh	15.93	4.81
Fine mesh	15.93	4.72

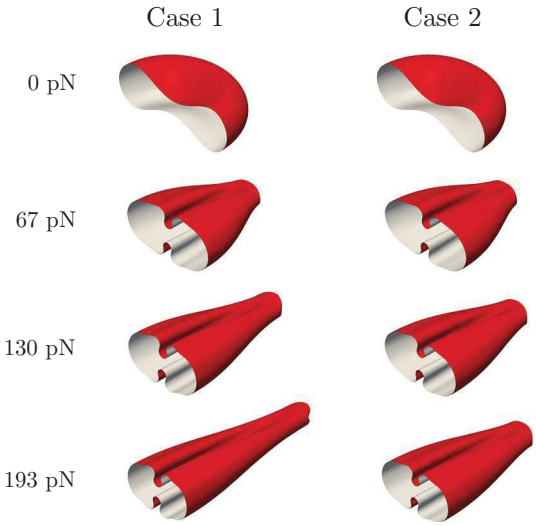

Fig. 3 Visualization of the red blood cell deformation over the entire range of stretching force, for both cases 1 and 2. Only half of the cell is displayed

4 Influence of the membrane modeling

The present computational setup is now used to investigate different continuum models of the RBC membrane. With the present numerical method, the different mechanical properties of the RBC membrane can be modeled by a combination of strain, area conservation and bending energies. Four new cases are summarized in Table 4.

Note that the bending stiffness of the lipid bilayer was neglected in cases 1 and 2, but is accounted for in the others. Using the Yeoh law (Eq. 2) to describe the local in-plane elasticity of the RBC membrane was seen to provide a good agreement with the optical tweezers experiment (see Fig. 2b). Case 3 thus appears to be a first obvious candidate to model the mechanics of the RBC membrane. As stated by Dimitrakopoulos (2012), the RBC membrane should rather be modeled by the Skalak law instead of the Yeoh law. Cases 4 and 5 are thus introduced, with two different values of the ratio C (low value in case 4, and high value in case 5). Note, however, that when using the Skalak law to model the local in-plane elasticity of the RBC membrane, a high value of C should be considered to restrain the area variations of the RBC membrane, thus modeling the quasi-incompressibility of the lipid bilayer. Consequently, case 4 does not constitute a potential candidate to model the mechanics of the RBC membrane, but is only introduced to investigate the influence of the ratio C on the mechanical response of the RBC subjected to optical stretching. Finally, case 6 proposes a hybrid modeling of the RBC membrane, dissociating the cytoskeleton and the lipid bilayer: The Skalak law with low ratio C is used to model the local in-plane elasticity of the cytoskeleton, allowing local area changes of the cytoskeleton; on top of this, the global area conservation energy is used to model the reorganisation of the quasi-incompressible lipid bilayer, sliding along the cytoskeleton. It is noticed that a twice smaller shear modulus E_s is considered when using the Skalak law in cases 4, 5 and 6, as compared to case 3. This factor of 2 is explained in the work of Dimitrakopoulos (2012) by the fact that the Yeoh and Skalak laws behave differently at moderate and high deformation. It is thus required to multiply the shear modulus E_s by 2 when considering the Yeoh law as compared to the Skalak law, in order to have a good comparison with the optical tweezers experiment in the large deformation range. Note that this results in an underestimation of the cell deformation for low stretching forces with the Yeoh law, as illustrated in the next section.

4.1 Comparison of axial and transverse diameters

Figure 4 shows the numerical predictions of the axial (D_A) and transverse (D_T) diameters for the different modeling cases introduced in Table 4. All cases provide a good comparison with the experimental results of Mills et al. (2004). Cases 5 and 6 are in a slightly better agreement with the experiment, especially regarding the transverse diameter (D_T) in the higher range of imposed stretching force. However, differences between all the modeling cases are contained within the experimental error bars.

It is interesting to note that increasing the resistance to area dilatation of the RBC membrane between case 4 and case 5 (by increasing the ratio C) has only a marginal influence on the predictions of the axial (D_A) and transverse (D_T) diameters, which was also observed in previous works (Sigüenza et al. 2014; Sinha and Graham 2015). In addition, restraining the area variation of the RBC membrane either locally (in case 5) or globally (in case 6) leads to almost identical predictions of the axial (D_A) and transverse (D_T) diameters.

4.2 Characterization of the RBC shape

The deformation of the stretched RBC at different stretching forces is displayed in Fig. 5. First, it is seen that the shapes obtained in case 3 differ from the ones obtained in case 2 (see Fig. 3), which also uses the Yeoh law to model the local in-plane elasticity of the RBC membrane. The large fold which appears during the RBC stretching in case 2 is

Table 4 Summary of different continuum models of the RBC membrane investigated by means of optical tweezers simulations (see Table 2 for cases 1 and 2)

	W		$\mathcal{E}_S$	$\mathcal{E}_b$
Case 3	YE:	$E_s = 7.3\ \mu$N/m $C_3 = E_s/30$	X	$\kappa_b = 2.0 \times 10^{-19}$ N.m
Case 4	SK:	$E_s = 3.65\ \mu$N/m $C = 0.5$	X	$\kappa_b = 2.0 \times 10^{-19}$ N.m
Case 5	SK:	$E_s = 3.65\ \mu$N/m $C = 100$	X	$\kappa_b = 2.0 \times 10^{-19}$ N.m
Case 6	SK:	$E_s = 3.65\ \mu$N/m $C = 0.5$	$\kappa_S = 1.0 \times 10^3\ \mu$N/m	$\kappa_b = 2.0 \times 10^{-19}$ N.m

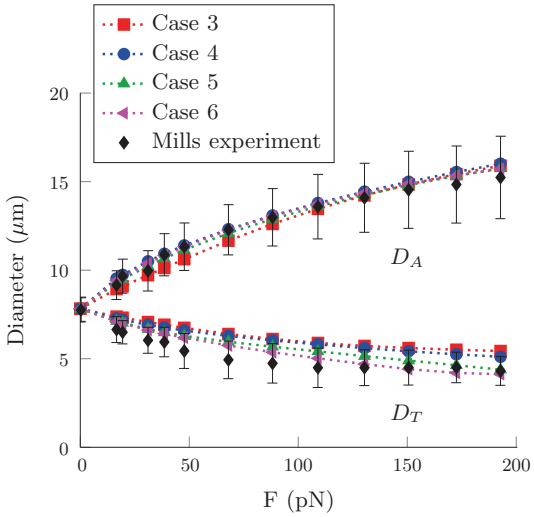

Fig. 4 Comparison of the axial (D_A) and transverse (D_T) diameters of the RBC stretched by optical tweezers for the different modeling cases introduced in Table 4

restrained in case 3 by the bending stiffness of the lipid bilayer, modeled by the bending energy (neglected in case 2). The fold is, however, still visible during the stretching, but much smoother. In case 4, when switching the hyperelastic model to the Skalak law, the RBC tends to lose its biconcave shape with increasing stretching. This phenomenon is even more pronounced and faster in case 5, when the area dilatation resistance is increased, leading to a more rounded shape at maximum stretching. Finally, case 6 exhibits a very similar behavior of case 5, with a faster transition from the biconcave to the rounded shape (see shapes at $F = 67$ pN in Fig. 5), and a more circular shape at maximum stretching. Note that simulations have also been performed combining the Yeoh law with the global area conservation energy, showing the same transition from the biconcave to the rounded shape (not shown). This indicates that this mechanical behavior does not come from the use of the Skalak law itself, but from the area variation restriction of the RBC membrane, achieved either using the Skalak law or the global area conservation energy.

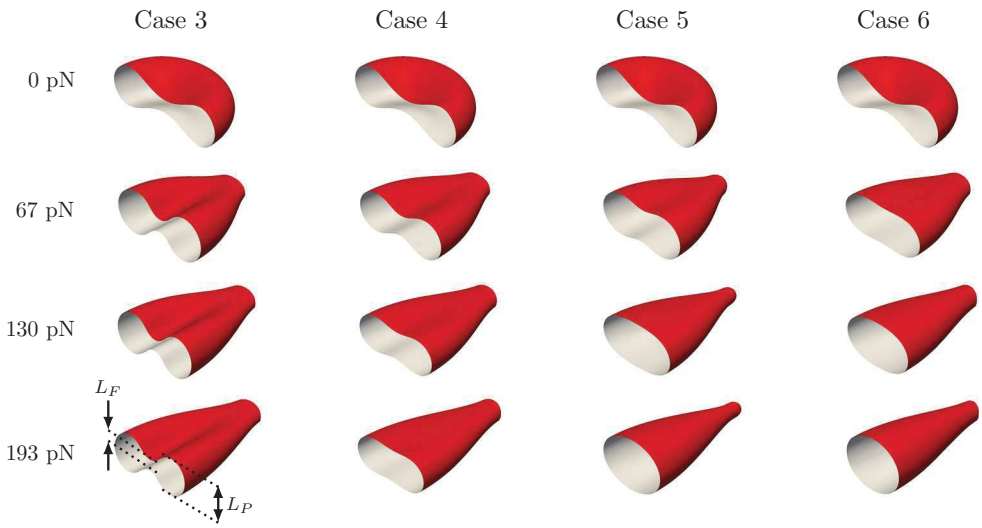

Fig. 5 Visualization of the red blood cell deformation over the entire range of stretching force, for the different modeling cases introduced in Table 4. Only half of the cell is displayed

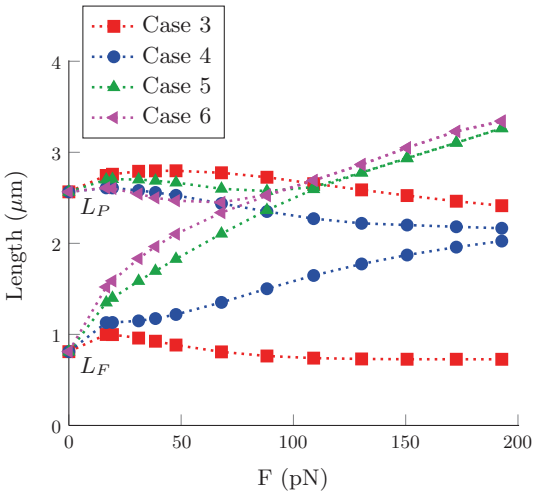

Fig. 6 Evolution of the in-plane (L_P) and folding (L_F) lengths for the different modeling cases introduced in Table 4

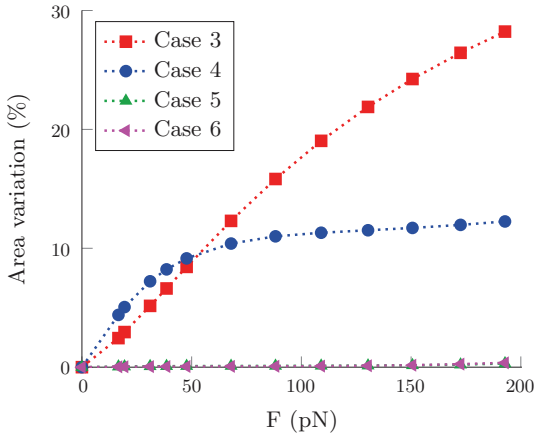

Fig. 7 Global area variation of the RBC membrane for the different modeling cases introduced in Table 4

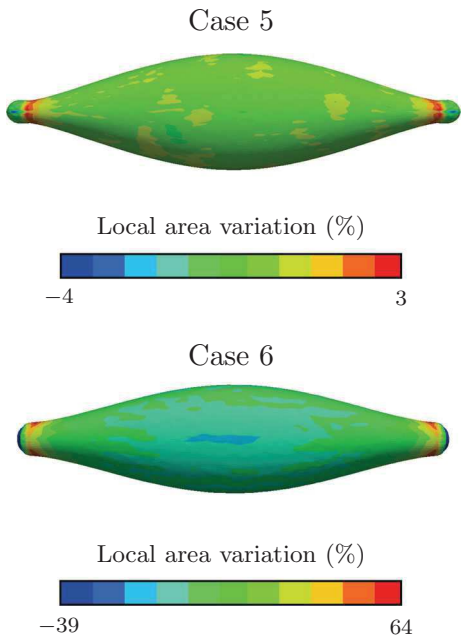

Fig. 8 Comparison of the local area variations of the red blood cell membrane at the maximum stretching force $F = 193$ pN, for the modeling approaches of cases 5 and 6

In the light of these observations, it appears relevant to introduce two additional lengths measured on the deformed RBC: The in-plane length L_P, defined as being the height in the direction perpendicular to the plane of the RBC (see Fig. 5); the folding length L_F, also aligned with the direction perpendicular to the plane of the RBC, but evaluated at the fold location (see Fig. 5). As shown in Fig. 6, the discrimination between the different modeling cases is more obvious when analyzing the evolution of the in-plane (L_P) and folding (L_F) lengths than the classical analysis made on the axial (D_A) and transverse (D_T) diameters (in Fig. 4). Previous observations of Fig. 5 can be highlighted: In case 3, the in-plane (L_P) and folding (L_F) lengths show parallel evolutions, meaning that the RBC keeps its biconcave shape for the whole range of stretching force; in case 4, lengths get closer with increasing stretching force, showing that the RBC progressively loses its biconcave shape when subjected to stretching; in cases 5 and 6, a transition from a biconcave folded shape to a rounded shape occurs when the two lengths become identical (for $F = 109$ pN in case 5, and $F = 88$ pN in case 6), and the shape of the RBC becomes more and more circular as the lengths increase with the stretching force.

4.3 Area variation

The ability of the quasi-incompressible lipid bilayer to restrain area variations during the RBC deformation is an important mechanical feature of the RBC membrane (Mohandas and Gallagher 2008). Figure 7 shows the evolution of the global area variation of the RBC membrane during stretching for the different modeling cases introduced in Table 4. In case 3, the area increase reaches 28%, since the Yeoh law is not designed to restrain area variations of the RBC membrane. Using the Skalak law in case 4 enables to restrain the area variation to a maximum value of 12%. Area variations are even more restrained when increasing the resistance to area dilatation in cases 5 (0.3%) and 6 (0.4%).

Figure 8 shows the local area variation of the RBC membrane for modeling cases 5 and 6. In case 5, the use of the Skalak law with high ratio C allows very small local area variations of the RBC membrane. In case 6, the quasi-incompressibility of the lipid bilayer is independently modeled using the global area conservation energy, whereas the Skalak law with lower ratio C is used to model the own area dilatation resistance of the cytoskeleton. This results in higher local area variations, which correspond to the defor-

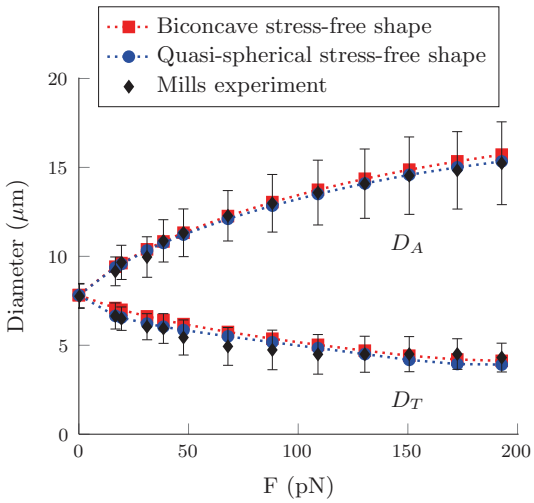

Fig. 9 Influence of the stress-free shape of the RBCs on the evolution of the axial (D_A) and transverse (D_T) diameters, for the modeling case 6

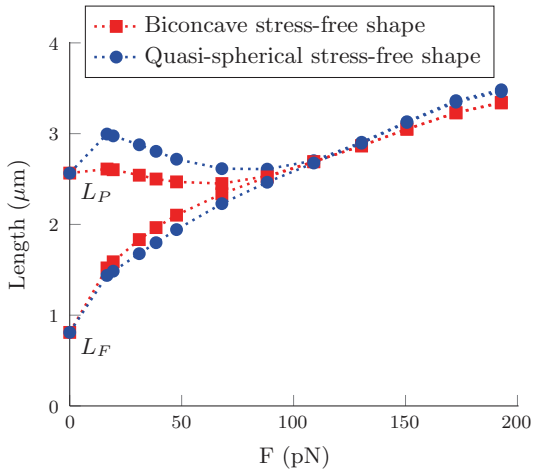

Fig. 10 Influence of the stress-free shape of the RBCs on the evolution of the in-plane (L_P) and folding (L_F) lengths, for the modeling case 6

mation of the cytoskeleton. In both cases, the maximum local area variations are obtained at the extremities of the cell, near to the bead/RBC contact areas. These regions of high stretching may thus be the locations where the RBC is the most prone to lysis. Note that variation of cytoskeleton area was measured by Discher et al. (1994) in a micropipette aspiration experiment, but the authors are not aware of similar measurements in optical tweezers experiment.

4.4 RBC stress-free shape

Recent studies suggest that RBCs have a quasi-spherical stress-free shape (Lim et al. 2002; Khairy and Howard 2011; Cordasco et al. 2014; Peng et al. 2014, 2015; Dupire et al. 2015), meaning that the well-known biconcave shape of the RBCs (Eq. 11) is pre-stressed. This initial pre-stress has not been taken into account so far in the present study, but could eventually play a significant role. Klöppel and Wall (2011) recently investigated the influence of an initial pre-stressed biconcave shape of a RBC subjected to stretching deformation, and almost no influence of this initial pre-stress was observed. They concluded that when investigating static deformation of RBCs, the biconcave initial shape of the RBCs can be assumed as being stress-free.

In this section, the influence of the quasi-spherical stress-free shape of the RBCs is investigated. Figure 9 compares previous simulations of the modeling case 6, assuming a biconcave stress-free shape of the RBC, with simulations where the stress-free shape of the RBC is a quasi-spherical shape having a reduced volume $V/V_0 = 0.98$ (with V_0 the volume of a sphere having the same surface area). As usually done when modifying the stress-free shape (Cordasco et al. 2014; Peng et al. 2014), the spontaneous curvature c_0 (Eq. 7) is adjusted so that the equilibrium shape is similar to the parametric biconcave shape described by Eq. (11). In the present case, the spontaneous curvature is set to $c_0 = 4.6 \times 10^6$ m^{-1}. Consistent with the conclusions made by Klöppel and Wall (2011), it is seen that there is no significant effect of the stress-free shape regarding the evolution of the axial (D_A) and transverse (D_T) diameters. Regarding the latter quantity, a slightly better agreement with the experiment is nonetheless observed when considering a quasi-spherical stress-free shape.

The evolution of the in-plane (L_P) and folding (L_F) lengths is displayed in Fig. 10, showing a more significant effect of stress-free shape. Indeed, it is seen that the in-plane length (L_P) is higher for the quasi-spherical stress-free shape before the transition from the biconcave to the rounded shape occurs.

5 Discussion

In the present paper, the optical tweezers experiment by Mills et al. (2004) is simulated using a numerical method dedicated to the simulation of the dynamics of RBCs under flow. A computational setup for simulating the RBC stretching is presented, which is seen to perfectly reproduce the numerical results obtained by Mills et al. (2004). Influence of the RBC membrane modeling is then investigated, introducing different continuum models to describe the membrane mechanics.

Comparison of the numerical results with the force-extension data provided by the experiment (i.e., the axial (D_A) and transverse (D_T) diameters of the stretched RBC) shows that all the considered modeling approaches are able to reproduce the mechanical response of the RBC subjected to optical stretching (see Fig. 4). An adjustment of the shear modulus E_s is, however, required depending if the RBC membrane is described using the Yeoh law or the Skalak

law (E_s is twice smaller when using the Skalak law). It is also seen that some of these models allow non-physiological area variations of the RBC membrane during stretching (see Fig. 7), especially the Yeoh law which was considered in previous works as a suitable model of the RBC membrane (Mills et al. 2004; Suresh et al. 2005). Consistent with the findings of Dimitrakopoulos (2012), this indicates that the Yeoh law should not be used to describe the mechanical behavior of the RBC membrane. This also indicates that the single analysis of the axial (D_A) and transverse (D_T) diameters of the stretched RBC is not sufficient for characterizing the mechanics of the RBC membrane, and cannot be used alone to validate numerical models of the RBC membrane.

Detailed analysis of the shape of the stretched RBC reveal different behaviors among the investigated models (see Fig. 5). A transition of the RBC shape from a biconcave folded shape to a rounded shape is observed when restraining the area variations of the RBC membrane, either locally or globally. This observation may be due to the fact that the RBC tends to lose its biconcave shape when subjected to optical stretching, to prevent area variations of the RBC membrane. Note that such ellipsoidal shapes were also reported in previous numerical studies (Li et al. 2005; Klöppel and Wall 2011; Farutin et al. 2014; Sigüenza et al. 2014).

This transition from a biconcave folded shape to a rounded shape can be characterized by introducing two additional measurements in the direction perpendicular to the plane of the RBC: The in-plane length L_P and the folding length L_F (see Fig. 6). Experimental measurements of such lengths could thus be of prime interest to make the optical tweezers experimental setup more helpful to characterize the mechanics of the RBC membrane. Indeed, these quantities reveal to be more sensitive to the area variation restriction of the RBC membrane than the usual force-extension data and could thus enable to better investigate the mechanical behavior of the membrane. Such data are also expected to be sensitive to the bending stiffness of the RBC membrane. However, the latter is seen to mainly influence the shape of the fold of the stretched RBC, but is not at the origin of the transition from the biconcave to the rounded shape. Indeed, this transition may occur even when the bending stiffness of the RBC membrane is not considered (Sigüenza et al. 2014). The lengths L_P and L_F are thus expected to be of interest to qualitatively challenge RBC modeling, while quantitative comparisons should account for the possible influence of the bending stiffness of the RBC membrane.

More sophisticated measurements of the shape of the stretched RBC must, however, be performed with reasonable experimental uncertainties. One of the main sources of uncertainty is expected to come from the contact areas between the beads and the RBC, which may vary from one experiment to the other. In the present computational setup, these contact areas are defined by the contact size d_c which

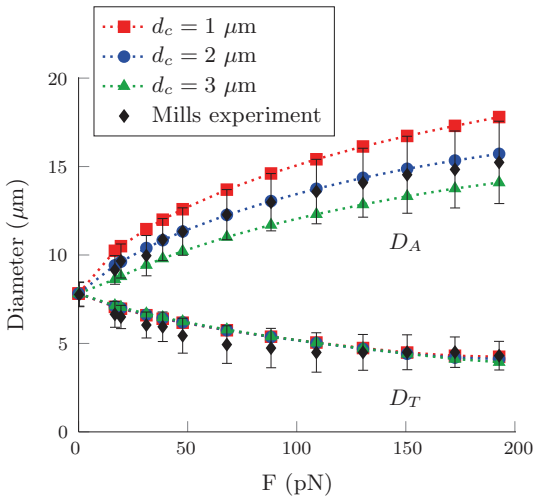

Fig. 11 Influence of the bead/RBC contact areas on the axial (D_A) and transverse (D_T) diameters, for the modeling case 6

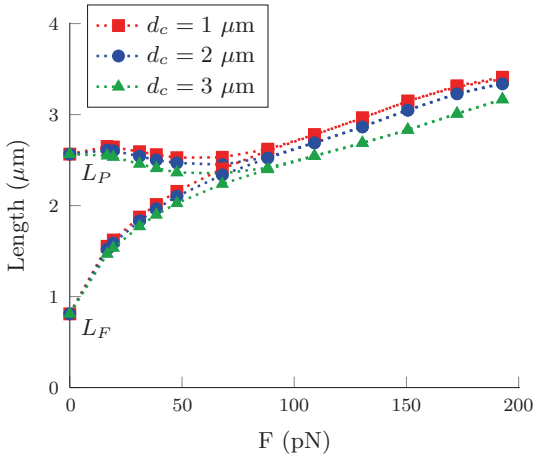

Fig. 12 Influence of the bead/RBC contact areas on the in-plane (L_P) and folding (L_F) lengths, for the modeling case 6

is initially chosen to be $d_c = 2\,\mu$m, as in the computations of Mills et al. (2004). Figure 11 shows the influence of this contact size on the numerical predictions of the axial (D_A) and transverse (D_T) diameters of the stretched RBC (using the modeling case 6), when the contact size is successively set to $d_c = 1\,\mu$m, $d_c = 2\,\mu$m and $d_c = 3\,\mu$m. It is seen that the contact size strongly influence the prediction of the axial diameter (D_A), showing a more rigid behavior with increasing d_c, but has no influence on the prediction of the transverse diameter (D_T). This may explain the large and increasing error bars obtained by Mills et al. (2004) in the experimental measurements of the axial diameter (D_A), as compared to the smaller and monotonous error bars obtained for the transverse diameter (D_T). This finding sheds doubt on the meaningfulness of the use of the axial diameter (D_A) for the determination of the shear modulus E_s. Indeed, the choice of the contact size d_c may strongly influence the

determined value of the shear modulus E_s. Conversely, simulations should rather be fitted to the transverse diameter (D_T) which is less sensitive to the choice of this contact size.

Figure 12 shows that the contact size d_c has only a little influence on the predictions of the in-plane (L_P) and folding (L_F) lengths, which means that comparison between computed and measured values of these quantities would be robust to the uncertainties related to the bead/RBC contact areas. The authors hope that these findings will arouse an interest for updated optical tweezers experiments.

Acknowledgements V. Moureau and G. Lartigue from the CORIA lab, and the SUCCESS scientific group are acknowledged for providing the YALES2 solver which constitutes the basis of the YALES2BIO tool.

Funding This study was performed with supports from ANR (FORCE project ANR-11-JS09-0011), from BPIfrance (DAT@DIAG Project No. I1112018W) and from the NUMEV Labex (ANR-10-LABX-20).

Compliance with ethical standards

Conflict of interest The authors declare that they have no conflict of interest.

References

Abkarian M, Viallat A (2016) Fluid–structure interactions in low-Reynolds-number flows. In: On the importance of the deformability of red blood cells in blood flow. Royal Society of Chemistry, London

Barthès-Biesel D, Diaz A, Dhenin E (2002) Effect of constitutive laws for two-dimensional membranes on flow-induced capsule deformation. J Fluid Mech 460:211–222

Charrier JM, Shrivastava S, Wu R (1989) Free and constrained inflation of elastic membranes in relation to thermoforming non-axisymmetric problems. J Strain Anal Eng Des 24(2):55–74

Chen M, Boyle FJ (2014) Investigation of membrane mechanics using spring networks: application to red-blood-cell modelling. Mater Sci Eng C 43:506–516

Chnafa C, Mendez S, Nicoud F (2014) Image-based large-eddy simulation in a realistic left heart. Comput Fluids 94:173–187

Chorin A (1968) Numerical solution of the Navier–Stokes equations. Math Comput 22:745–762

Cordasco D, Yazdani Bagchi P (2014) Comparison of erythrocyte dynamics in shear flow under different stress-free configurations. Phys Fluids 26:041902

Dao M, Lim CT, Suresh S (2003) Mechanics of the human red blood cell deformed by optical tweezers. J Mech Phys Solids 51:2259–2280

Dao M, Li J, Suresh S (2006) Molecularly based analysis of deformation of spectrin network and human erythrocyte. Mater Sci Eng C 26:1232–1244

Dimitrakopoulos P (2012) Analysis of the variation in the determination of the shear modulus of the erythrocyte membrane: effects of the constitutive law and membrane modeling. Phys Rev E 85:041917

Discher DE, Mohandas N, Evans EA (1994) Molecular maps of red cell deformation: hidden elastic and in situ connectivity. Science 266:1032–1035

Doddi SK, Bagchi P (2008) Lateral migration of a capsule in a plane Poiseuille flow in a channel. Int J Multiph Flow 34:966–986

Dupire J, Abkarian M, Viallat A (2015) A simple model to understand the effect of membrane shear elasticity and stress-free shape on the motion of red blood cells in shear flow. Soft Matter 11:8372–8382

Eggleton CD, Popel AS (1998) Large deformation of red blood cell ghosts in a simple shear flow. Phys Fluids 10(8):1834–1845

Evans EA (1973) New membrane concept applied to the analysis of fluid shear- and micropipette-deformed red blood cells. Biophys J 13:941–954

Evans EA, Fung YC (1972) Improved measurements of the erythrocyte geometry. Microvasc Res 4:335–347

Farutin A, Biben T, Misbah C (2014) 3D numerical simulations of vesicle and inextensible capsule dynamics. J Comput Phys 275:539–568

Fedosov DA, Caswell B, Karniadakis G (2010a) Systematic coarse-graining of spectrin-level red blood cell models. Comput Methods Appl Mech Eng 199:1937–1948

Fedosov DA, Caswell B, Karniadakis GE (2010b) A multiscale red blood cell model with accurate mechanics, rheology, and dynamics. Biophys J 98:2215–2225

Fedosov DA, Noguchi H, Gompper G (2014) Multiscale modeling of blood flow: from single cells to blood rheology. Biomech Model Mechanobiol 13:239–258

Helfrich W (1973) Elastic properties of lipid bilayers: theory and possible experiments. Z Naturforsch 28c:693–703

Hénon S (1999) A new determination of the shear modulus of the human erythrocyte membrane using optical tweezers. Biophys J 76:1145–1151

Khairy K, Howard J (2011) Minimum-energy vesicle and cell shapes calculated using spherical harmonics parameterization. Soft Matter 7:2138–2143

Klöppel T, Wall WA (2011) A novel two-layer, coupled finite element approach for modeling the nonlinear elastic and viscoelastic behavior of human erythrocytes. Biomech Model Mechanobiol 10:445–459

Le DV, White J, Peraire J, Lim KM, Khoo BC (2009) An implicit immersed boundary method for three-dimensional fluid–membrane interactions. J Comput Phys 228:8427–8445

Li J, Dao M, Lim CT, Suresh S (2005) Spectrin-level modeling of the cytoskeleton and optical tweezers stretching of the erythrocyte. Biophys J 88:3707–3719

Lim GHW, Wortiz M, Mukhopadhyay R (2002) Stomatocyte-discocyte-echinocyte sequence of the human red blood cell: evidence for the bilayer-couple hypothesis from membrane mechanics. Proc Natl Acad Sci USA 99(26):16,766–16,769

Lim GHW, Wortiz M, Mukhopadhyay R (2008) Red blood cell shapes and shape transformations: Newtonian mechanics of a composite membrane, soft matter, vol lipid bilayers and red blood cells, chap 2. WILEY-VCH Verlag GmbH & Co. KGaA, Weinheim

Malandain M, Maheu N, Moureau V (2013) Optimization of the deflated conjugate gradient algorithm for the solving of elliptic equations on massively parallel machines. J Comput Phys 238:32–47

Martins Afonso M, Mendez S, Nicoud F (2014) On the damped oscillations of an elastic quasi-circular membrane in a two-dimensional incompressible fluid. J Fluid Mech 746:300–331

Mendez S, Gibaud E, Nicoud F (2014) An unstructured solver for simulations of deformable particles in flows at arbitrary Reynolds numbers. J Comput Phys 256(1):465–483

Mills JP, Qie L, Dao M, Lim CT, Suresh S (2004) Nonlinear elastic and viscoelastic deformation of the human red blood cell with optical tweezers. Mech Chem Biosyst 1(3):169–180

Mohandas N, Gallagher PG (2008) Red cell membrane: past, present, and future. Blood 112(10):3939–3948

Moureau V, Domingo P, Vervisch L (2011) Design of a massively parallel CFD code for complex geometries. Comp Rend Méc 339(2–3):141–148

Peng Z, Mashayekh A, Zhu Q (2014) Erythrocyte responses in low-shear-rate flows: effects of non-biconcave stress-free state in the cytoskeleton. J Fluid Mech 742:96–118

Peng Z, Salehyar S, Zhu Q (2015) Stability of the tank treading modes of erythrocytes and its dependence on cytoskeleton reference states. J Fluid Mech 771:449–467

Peskin CS (2002) The immersed boundary method. Acta Number 11:479–517

Pinelli A, Naqavi IZ, Piomelli U, Favier J (2010) Immersed-boundary methods for general finite-difference and finite-volume Navier–Stokes solvers. J Comput Phys 229:9073–9091

Pivkin IV, Karniadakis GE (2008) Accurate coarse-grained modeling of red blood cells. Phys Rev Lett 101:118105

Sigüenza J, Mendez S, Nicoud F (2014) Characterisation of a dedicated mechanical model for red blood cells: numerical simulations of optical tweezers experiment. Comput Methods Biomech Biomed Eng 17(supp. 1):28–29

Sigüenza J, Mendez S, Ambard D, Dubois F, Jourdan F, Mozul R, Nicoud F (2016) Validation of an immersed thick boundary method for simulating fluid–structure interactions of deformable membranes. J Comput Phys 322:723–746

Sinha K, Graham MD (2015) Dynamics of a single red blood cell in simple shear flow. Phys Rev E 92:042710

Skalak R, Tozeren A, Zarda RP, Chien S (1973) Strain energy function of red blood cell membranes. Biophys J 13:245–264

Sui Y, Chew YT, Roy P, Cheng YP, Low HT (2008) Dynamic motion of red blood cells in simple shear flow. Phys Fluids 20:112106

Suresh S, Spatz J, Mills JP, Micoulet A, Dao M, Lim CT, Beil M, Seufferlein T (2005) Connections between single-cell biomechanics and human disease states: gastrointestinal cancer and malaria. Acta Biomater 1:15–30

Yeoh OH (1993) Some forms of the strain energy function for rubber. Rubber Chem Technol 66(5):754–771

Zhong-can OY, Helfrich W (1989) Bending energy of vesicle membranes: general expressions for the first, second, and third variation of the shape energy and applications to spheres and cylinders. Phys Rev A 39(10):5280–5288

Zmijanovic V, Mendez S, Moureau V, Nicoud F (2017) About the numerical robustness of biomedical benchmark cases: interlaboratory FDA's idealized medical device. Int J Numer Methods Biomed Eng 33(1):1–17